Experimental study on the buckling resistance of cold-formed steel back-to-back plain and lipped channels in bending

Ungureanu, Viorel; Both, Ioan; Bodea, Florin; Lukačević, Ivan

Experimental study on the buckling resistance of cold-formed steel back-to-back plain and lipped channels in bending

Viorel Ungureanu[1], Ioan Both[2], Florin Bodea[3], Ivan Lukačević[4]

Abstract

Cold-formed steel profiles are increasingly in demand in the construction market because of their speed of assembly and low material consumption. Thus, it is necessary to investigate their behavior in depth, since in recent years they have been used as the main structural components of buildings. The paper presents an experimental program where several types of built-up section configurations were tested made of lipped or plain channels, such as simple built-up back-to-back (SBB) and back-to-back with spacers (BBS) cross-sections and two types of discrete connections, i.e. bolts and spot welding. The paper is based on a previous parametric numerical investigation performed to identify the influence of several parameters, i.e. the type of the channel section, length of the beam, continuous and discrete connections between channels, the number and the distance between discrete connections along the beam axis and along the beam height. From the parametric study, it was concluded that the capacity of the cold-formed steel back-to-back built-up steel beams is highly affected by the type of connections. The static scheme of the beams used the 4-point bending setup so that the central area is subject only to the bending moment. The length between the loading points was monitored to capture the behavior of the beams from local to distortional and interactive buckling. A total of thirty beams subjected to pure bending with built-up sections were tested. In addition, the out-of-plane displacements were restricted at the loading points to control the failure area. Before the tests were performed, the sectional dimensions and imperfections of the elements were measured, as this represents a critical issue in the behavior of thin-walled cold-formed steel elements. A 3D laser scanner was used to determine the initial imperfections. The records allowed measurement of the initial imperfections in relation to the nominal cross-section.

1. Introduction

Cold-formed steel (CFS) sections have limited capacity because of their instability problems and one of the ways to increase their resistance is by fabricating built-up sections. A built-up cross-section with discrete connections along the length may fail as failure of the individual members or buckling in interaction modes depending on the intermediate connection type, spacing and slenderness. Commonly connected by screws, the rigidity of such connection is small, thus the need for a more rigid fastening (such as bolts or spot welding) and more consistent in terms of repeatability.

Although design methods are established for traditional cold-formed steel open sections, the design methods for the built-up cross-sections are currently under investigation.

Knowing the instability problems that occur, most of the experimental work on built-up cross-sections was focused on centric compression of studs either with open sections [1,2,3], or closed sections [4,5,6]. Built-up open section members under eccentric compressive load were also investigated to assess their strengths [7]. The investigations mentioned above found that the design methods underestimate the strength in both compressed and eccentrically compressed elements.

Ye et al. [8,9] describe an experimental program to investigate the interaction of local and distortional buckling in cold-formed steel lipped channel beams, including three different cross-sectional geometries. Comparisons showed good agreement between the experimental results and the predictions of the European design guidelines and current North American provisions, while other DSM formulations resulted in rather conservative predictions. Li and Young [10] performed a series of tests on built-up steel sections with nonuniform bending that showed the conservative strength prediction of AISI S100 [11], AS/NZS 4600 [12], EN

1993-1-1 [13] and ANSI / ASC 360 [14] design methods for open cross-section and slightly conservative strength prediction for closed sections.

Thus, there is a need for more experimental tests to cover the connection type, spacing and slenderness. This study aims to enlarge the experimental database of built-up back-to-back elements subjected to bending, covering all possible failure modes, local, distortional and interactive buckling, considering fastenings with higher rigidity compared to the screwed connection, and in direct contact or distanced by a spacer configuration. A total of thirty specimens were tested, considering lipped and plain cross-sections, connected with bolts or by spot welding.

2. Experimental program

The experimental program on back-to-back built-up members within the CFS Expert research project comprised 30 beam typologies for elements subjected to bending moment, considering the quasi-static loading rate protocol. The specimens were selected based on a previous parametric numerical investigation performed to identify the influence of several parameters, i.e. the type of channel section, the length of the beam, continuous and discrete connections between channels, the number and distance between discrete connections along the beam axis and along the height of the beam [15].

2.1 Specimens

Two identical sections of CFS profiles were connected in a back-to-back configuration considering the direct connection of the profiles or using spacers between the profiles at every 30 cm. Four sections were used to obtain the desired configurations as nominally presented in Figure 1, considering the values presented in Table 1.
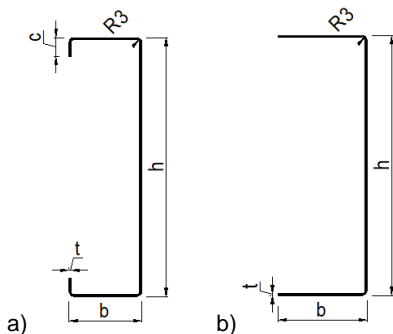

Figure 1: Nominal dimensions a) C profile, b) U profile

With these sections, considering the distances between the load application points, different failure modes were expected to be found, that is, local (L), distortional (D), or interactive (G) buckling.

Table 1: Dimensions of the profiles

Specimen	h [mm]	b [mm]	t_{nom} [mm]	c [mm]	R [mm]
C200	200	45	1.5	13	3
C240	240	70	2.0	18	3
U200	203	53	1.5	-	4
U240	244	85	2.0	-	4

To connect the profiles, two different techniques were used i.e. bolts (B) and spot welding (SW). For the bolted specimens, M12 bolts were used. To increase the certainty of the results, some typologies were tested twice.

The name of the specimens represents a format that includes the parameters of the specimens presented above, 2V-W-X-Y-Z_N indicating the 2 profiles, V - the profile shape (U or C), W - connection type (B or SW), X - type of the profile (200 or 240), Y - the thickness of the profile (1.5 or 2.0), Z - expected failure mode (L, D, or I), N - number of the specimen. As an example, 2C-B-200-1.5-L_1 represents a built-up section of two lipped channels, connected by bolts, with a profile of 200mm, a thickness of 1.5mm, expected to present deformations characteristic to the local failure mode, being the first specimen of the series. A series of specimens were built-up with a space of 75mm between the profiles, using a C75 lipped channel section as a spacer. The name of these specimens additionally includes the "St" (Stitch) nomination.

Before proceeding to testing, the real dimensions of the sections were measured. The values presented represent the average of the measurements taken at every 500mm along the specimen, for both the back and front profiles (see Tables 2 to 5). The nomenclature for the real dimensions is presented in Figure 2, where *ba* and *fr* represent the back and front profiles.
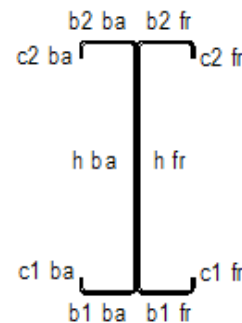

Figure 2: Nomenclature for the real dimensions

Knowing the sensitivity of thin-walled CFS members to imperfections, a portable 3D laser scanner (HandySCAN3D) from CREAFORM was used (the linear accuracy is 0.025mm and the volumetric one is 0.020 + 0.040mm/m). The recordings allowed the measurement of the imperfection and dimensions with respect to the ideal cross-

section. An example of the procedure is shown in Figure 3, where the scanned model is superimposed on the ideal model so that the deviation of the specimen from the ideal section can be observed. Individual profiles were initially scanned and then connected, resulting in a composite beam that was also scanned.

Table 2: Real dimensions for the front U profiles

Specimen	h [mm]	b_1 [mm]	b_2 [mm]	t [mm]	Zn [µm]
2U-B-200-15-L_2	203.36	49.16	54.34	1.51	15.19
2U-B-200-15-G_1	203.37	50.37	53.06	1.52	13.28
2U-SW-200-15-L_1	203.40	48.90	54.62	1.52	15.64
2U-SW-200-15-G_1	203.37	49.03	54.42	1.50	13.53
2U-St-B-200-15-L_1	203.41	52.05	51.37	1.50	14.74
2U-St-B-200-15-G_1	203.37	49.03	54.42	1.50	13.53
2U-B-240-20-L_2	245.27	81.18	82.72	2.00	14.81
2U-B-240-20-G_1	245.61	80.83	82.81	1.99	12.58
2U-SW-240-20-L_1	245.74	80.60	83.20	1.99	13.59
2U-SW-240-20-G_1	245.56	81.34	82.66	1.99	13.25
2U-St-B-200-15-L_1	245.35	81.11	82.83	1.99	15.64
2U-St-B-200-15-G_1	245.56	82.85	81.02	1.98	15.75

Table 3: Real dimensions for the back U profiles

Specimen	h [mm]	b_1 [mm]	b_2 [mm]	t [mm]	Zn [µm]
2U-B-200-15-L_2	203.42	48.64	54.73	1.49	15.06
2U-B-200-15-G_1	203.48	50.46	52.94	1.51	13.93
2U-SW-200-15-L_1	203.36	48.56	54.91	1.52	16.74
2U-SW-200-15-G_1	203.29	48.94	54.54	1.50	14.20
2U-St-B-200-15-L_1	203.35	50.99	52.45	1.54	13.50
2U-St-B-200-15-G_1	203.29	48.94	54.54	1.50	14.20
2U-B-240-20-L_2	245.34	81.14	82.74	2.00	15.14
2U-B-240-20-G_1	245.76	80.97	82.80	1.99	12.41
2U-SW-240-20-L_1	245.80	80.52	83.29	2.00	12.69
2U-SW-240-20-G_1	245.58	80.96	82.91	1.99	12.77
2U-St-B-200-15-L_1	245.31	81.04	82.88	1.99	15.27
2U-St-B-200-15-G_1	245.49	82.86	81.08	1.99	16.55

Table 4: Real dimensions for the front C profiles

| Specimen	h [mm]	b_1 [mm]	b_2 [mm]	c_1 [mm]	c_2 [mm]	t [mm]	Zn [µm]
2C-B-200-15-L_1	199.37	43.55	45.52	11.43	12.88	1.50	15.19
2C-B-200-15-D_1	199.41	43.59	45.40	11.37	12.95	1.51	13.27
2C-B-200-15-G_1	199.35	43.75	45.29	11.40	13.00	1.49	12.06
2C-SW-200-15-L_1	199.29	43.51	45.54	11.33	13.12	1.52	17.34
2C-SW-200-15-D_1	199.30	43.49	45.45	11.38	13.11	1.50	14.76
2C-SW-200-15-G_1	199.52	44.81	44.28	13.48	10.80	1.51	14.54
2C-St-B-200-15-L_1	199.39	43.44	45.59	11.44	13.35	1.50	13.54
2C-St-B-200-15-D_1	199.33	43.58	45.32	11.48	13.03	1.50	11.53
2C-St-B-200-15-G_1	199.39	43.64	45.37	11.53	12.88	1.50	11.71
2C-B-240-20-L_2	239.99	69.11	71.96	15.73	18.00	1.99	17.70
2C-B-240-20-D_1	239.78	69.22	71.92	15.84	17.97	1.98	16.03
2C-B-240-20-G_1	293.33	85.41	87.93	19.05	21.50	1.98	19.43
2C-SW-240-20-L_1	240.60	69.28	70.20	20.27	14.90	2.00	20.34
2C-SW-240-20-D_1	240.19	69.43	71.27	14.86	19.19	1.97	15.81
2C-SW-240-20-G_1	240.10	71.91	69.21	18.39	15.20	1.99	17.24
2C-St-B-200-15-L_1	239.69	70.92	71.76	14.47	18.05	2.00	14.40
2C-St-B-200-15-D_1	239.81	70.96	72.08	14.57	17.48	2.00	14.32
2C-St-B-200-15-G_1	240.00	69.88	71.94	15.59	17.59	1.98	15.90

a)

b)
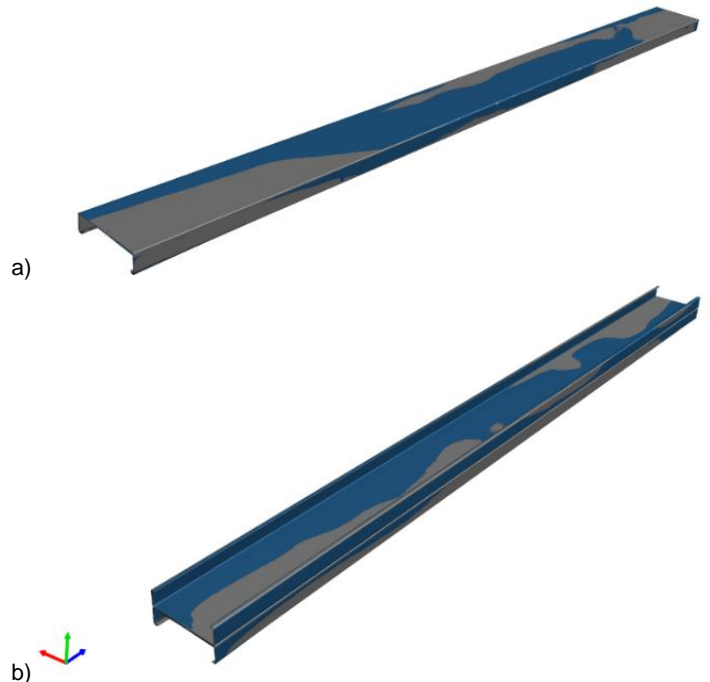
Figure 3: Overlap of the scanned shape with the reference model. a) individual elements, b) built-up specimen
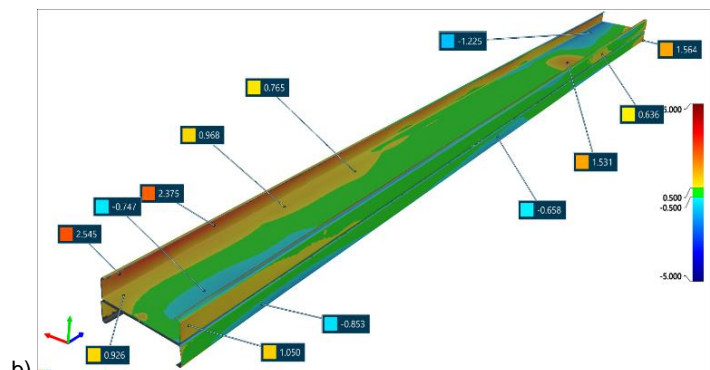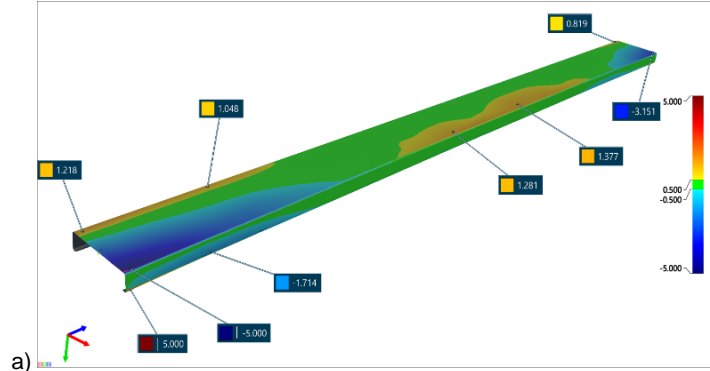

a)

b)

Figure 4: Overlap of the scanned shape with the reference model. a) individual elements, b) built-up specimen

Table 5: Real dimensions for the back C profiles

Specimen	h [mm]	b_1 [mm]	b_2 [mm]	c_1 [mm]	c_2 [mm]	t [mm]	Zn [µm]
2C-B-200-15-L_1	199.41	43.50	45.42	11.58	12.85	1.50	15.59
2C-B-200-15-D_1	199.36	43.63	45.37	11.45	12.82	1.50	13.21
2C-B-200-15-G_1	199.39	43.59	45.31	11.44	12.97	1.50	13.67
2C-SW-200-15-L_1	199.35	43.54	45.51	11.31	13.11	1.52	17.13
2C-SW-200-15-D_1	199.35	43.51	45.18	11.35	13.15	1.51	15.44
2C-SW-200-15-G_1	199.52	45.18	43.78	13.22	11.12	1.52	15.28
2C-St-B-200-15-L_1	199.38	43.47	45.38	11.41	13.26	1.50	13.41
2C-St-B-200-15-D_1	199.23	43.50	45.49	11.35	13.08	1.50	11.10
2C-St-B-200-15-G_1	199.39	43.74	45.29	11.44	12.97	1.49	12.88
2C-B-240-20-L_2	240.03	69.20	71.87	15.72	17.97	2.00	17.06
2C-B-240-20-D_1	239.7	69.21	71.90	15.90	17.84	1.98	15.24
2C-B-240-20-G_1	239.24	84.56	87.85	19.55	21.80	1.98	18.40
2C-SW-240-20-L_1	240.43	69.68	70.06	20.05	14.90	2.00	19.79
2C-SW-240-20-D_1	240.20	69.55	71.69	14.60	18.91	1.97	15.56
2C-SW-240-20-G_1	239.99	71.96	69.18	18.05	15.62	1.99	16.69
2C-St-B-200-15-L_1	239.66	70.97	71.72	14.43	18.04	2.00	16.86
2C-St-B-200-15-D_1	239.78	71.00	71.83	14.63	17.80	2.00	14.25
2C-St-B-200-15-G_1	239.93	69.19	71.88	15.99	17.84	1.98	15.05

2.2 Base material

The properties of the material were determined from tensile tests, according to [16], prior to beam testing, on three specimens extracted from the flange and the web. The C200 and U200 were formed from the same width of steel sheet, while the material for C240 and U240 had different properties. The engineering stress-strain curves are presented in U200, C240 and U240 in Figures 5 to 7 and the mechanical properties of the base material are presented in Table 6.
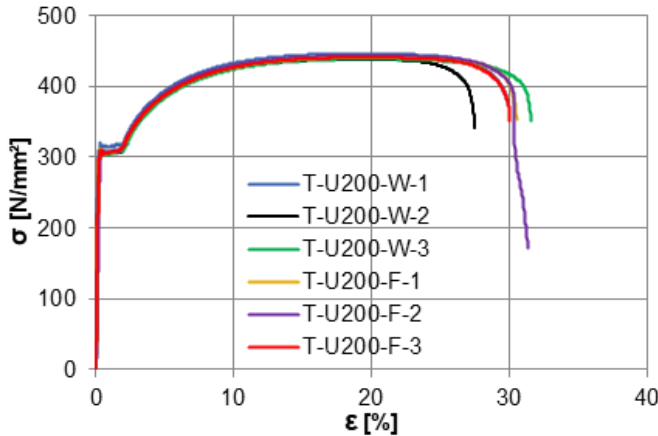

Figure 5: Stress - Strain curves for C200 and U200 base material

Table 6: Base material mechanical properties

Specimen	$R_{p0.2}$ (MPa)	R_m (MPa)	A_g %	A_t %
U200 (C200)	315	440	19.4	23.9
C240	370	525	15.0	26.3
U240	353	492	15.3	27.7

where:
$R_{p0.2}$ - stress at 0.2% strain
R_m - stress corresponding to the maximum force
A_{gt} - total extension at maximum force
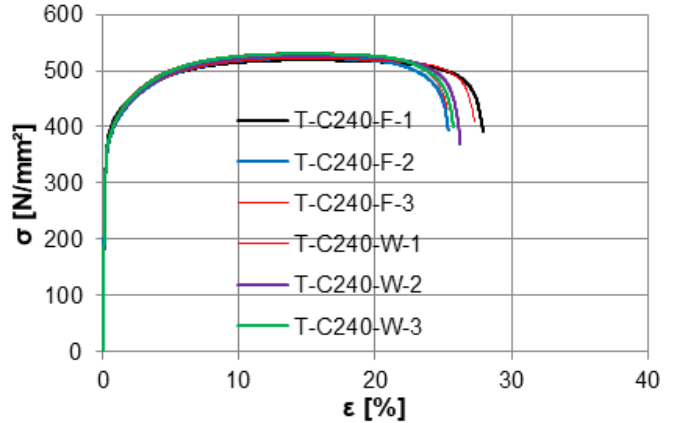A_t - total extension at the moment of fracture

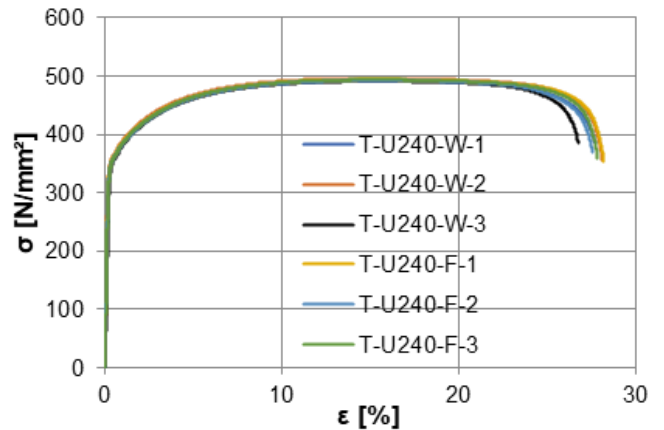Figure 6: Stress - Strain curves for C240 base material

Figure 7: Stress - Strain curves for U240 base material

Figure 8: Tensile specimens after the test

2.3 Testing

In order to carry out the experimental tests, an experimental stand was set up within the CEMSIG Research Center of the Department of Steel Structures and Structural Mechanics.

4

The test setup consists of the main frame with a 500kN actuator equipped with a force cell and displacement transducer fixed on the beam and a secondary frame for lateral bracing to avoid lateral torsional buckling of the elements in bending.
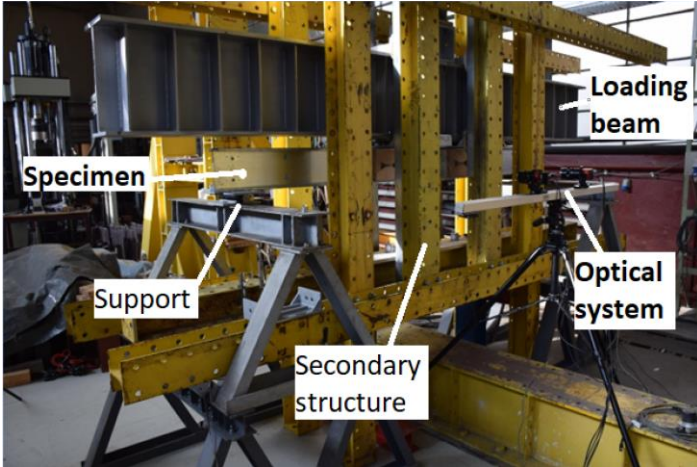

Figure 9: Experimental test setup

The elements were loaded in a 4-point bending configuration (see Figure 10), leading to a central area subjected only to the bending moment. The lengths of the specimens, L, the distance between the concentrated forces and supports, L_1, and the length between the loading points, L_2, are presented in Table 7.
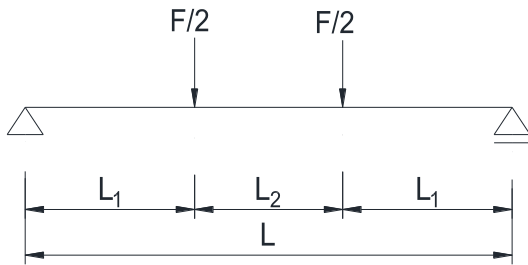
Figure 10: Loading configuration

The length L_2 was chosen to develop the desired instability, i.e. local, distortional, or interactive global buckling.

A total of eight displacement transducers were installed to monitor the displacements of the beams, that is, supports (2 vertical, 2 horizontal), load application points (1 vertical for each point), and midspan (2 vertical).

The imperfection measurements for the webs in bending have been performed using "isi SYS GmbH" Digital Image Correlation systems. During the tests, the beams were also monitored using the same optical system that can provide data to determine the strains as presented in Figure 9 (Digital Image Correlation technique).

Table 7: Distances of loading configurations

Specimen	L (mm)	L_1 (mm)	L_2 (mm)
2C-B-200-15-D	3200	1000	1200
2C-B-200-15-G	3800	1000	1800
2C-B-200-15-L	2600	1000	600
2C-B-240-20-D	4000	1000	2000
2C-B-240-20-G	5000	1000	3000
2C-B-240-20-L	2600	1000	600
2C-SW-200-15-D	3200	1000	1200
2C-SW-200-15-G	4000	1100	1800
2C-SW-200-15-L	2600	1000	600
2C-SW-240-20-D	4000	1000	2000
2C-SW-240-20-G	5000	1100	2800
2C-SW-240-20-L	2600	1000	600
2C-St-B-200-15-D	3200	1000	1200
2C-St-B-200-15-G	3800	1000	1800
2C-St-B-200-15-L	2600	1000	600
2C-St-B-240-20-D	4400	1000	2400
2C-St-B-240-20-G	5000	1000	3000
2C-St-B-240-20-L	2600	1000	600
2U-B-200-15-G	3800	1000	1800
2U-B-200-15-L	2600	1000	600
2U-B-240-20-G	5200	1000	3200
2U-B-240-20-L	2600	1000	600
2U-SW-200-15-G	4200	1200	1800
2U-SW-200-15-L	2600	1000	600
2U-SW-240-20-G	5200	1000	3200
2U-SW-240-20-L	2600	1000	600
2U-St-B-200-15-G	4200	1000	2200
2U-St-B-200-15-L	2600	1000	600
2U-St-B-240-20-G	5200	1200	2800
2U-St-B-240-20-L	2600	1000	600

3. Results

The following chapters will present the deformed shape of the elements for each expected failure mode, the initial shape of the web monitored with the optical system, and the force-displacement curves obtained from the actuator.

Of course, the capacity is influenced by the cross-sectional properties, but, qualitatively, similarities are observed for the same groups of failures and testing configurations.

Regardless of the C-profile dimensions, the short specimens tested, with small distances between the loading points, exhibited an interactive local-distortional buckling, and finally, due to the localization of the buckling modes a distortional plastic mechanism is observed. The failure shape is very similar to a very slender double-T steel profile, Figure 11a.

The specimens expected to fail in a distortional buckling (D), clearly formed the half-wave lengths, which, at excessive stress, are transformed into a localized mechanism.

The maximum moment of the tested specimens and the failure modes are summarized in Table 8.

3.1 Built-up beams with bolts of C200x1.5 profiles

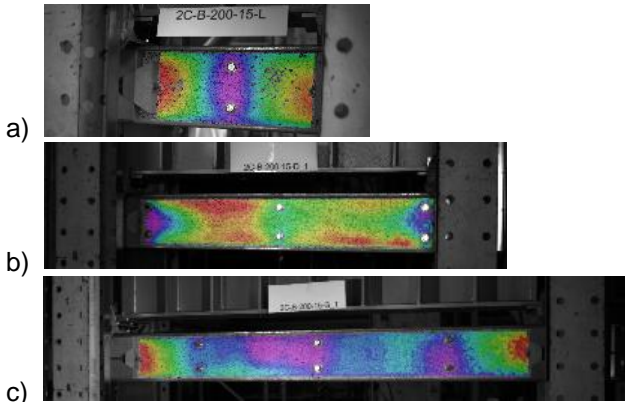Figure 11: Deformations for 2C-B-200-1.5 a) Local, b) Distortional, c) Interactive buckling

Figure 12: Initial imperfections for 2C-B-200-1.5 a) Local, b) Distortional, c) Interactive buckling
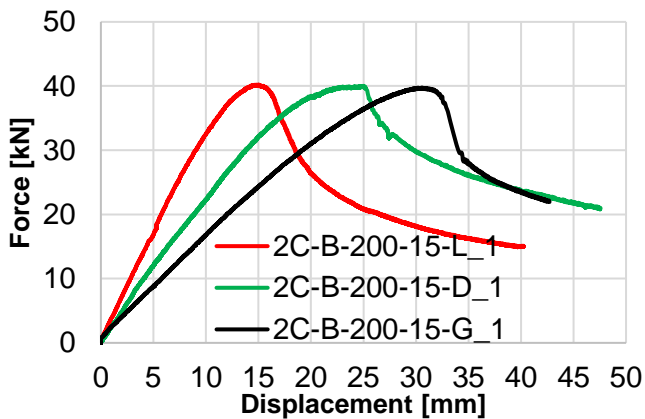

Figure 13: Force-Displacement curves for 2C-B-200-1.5
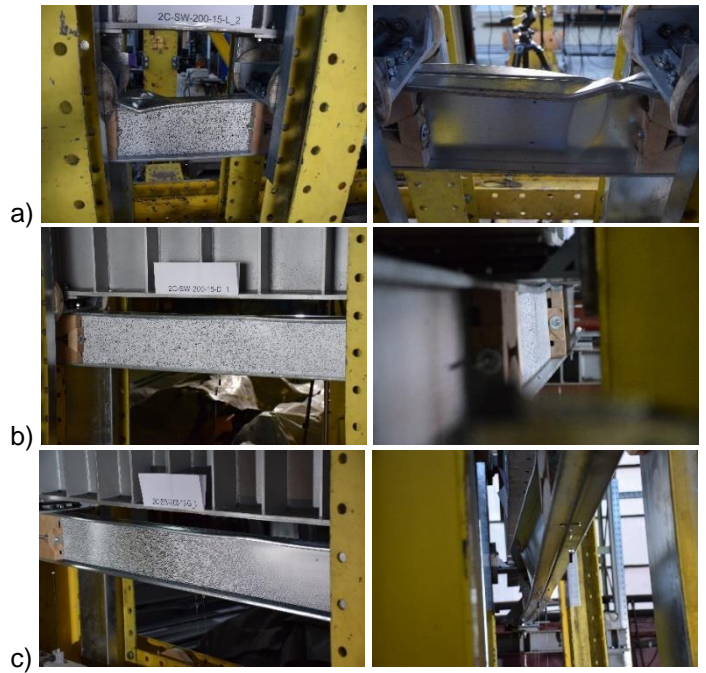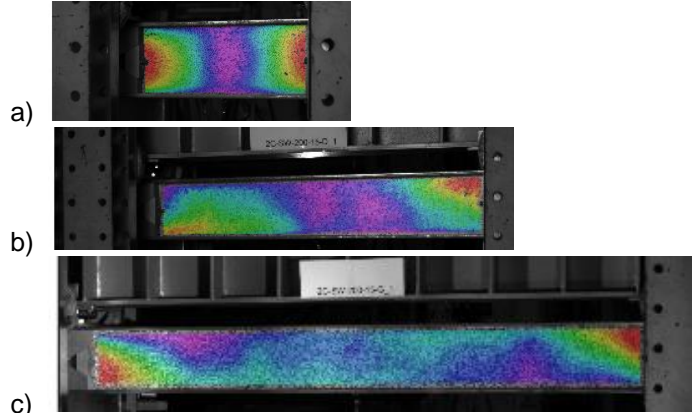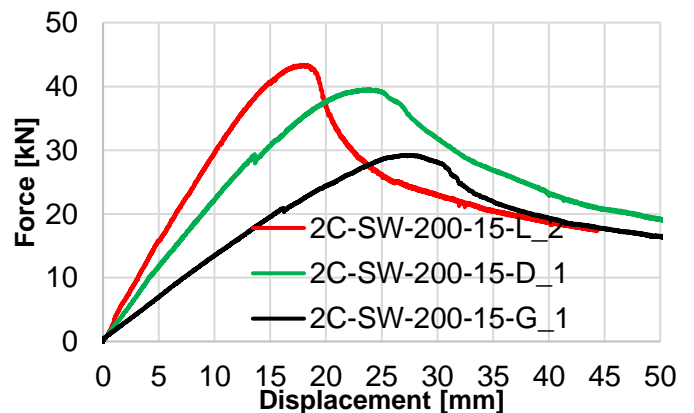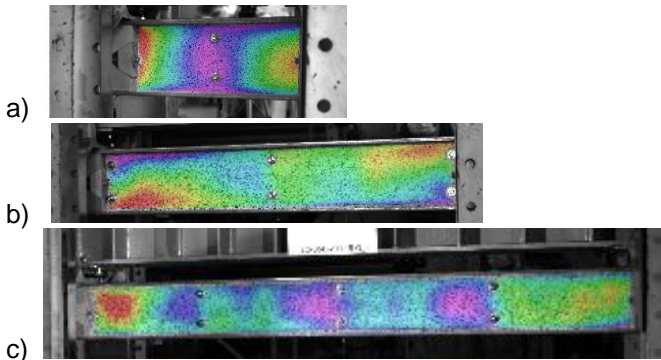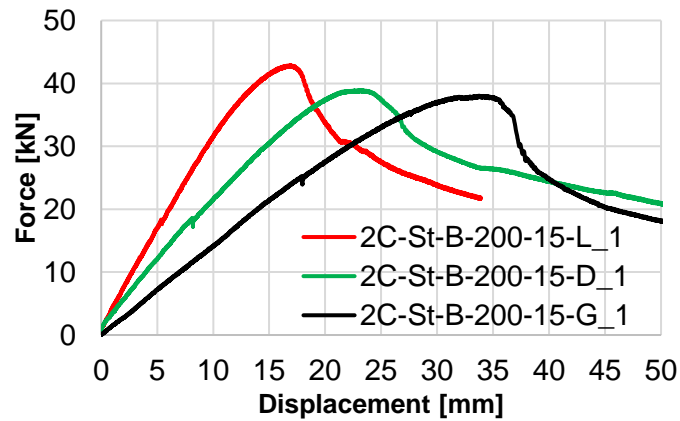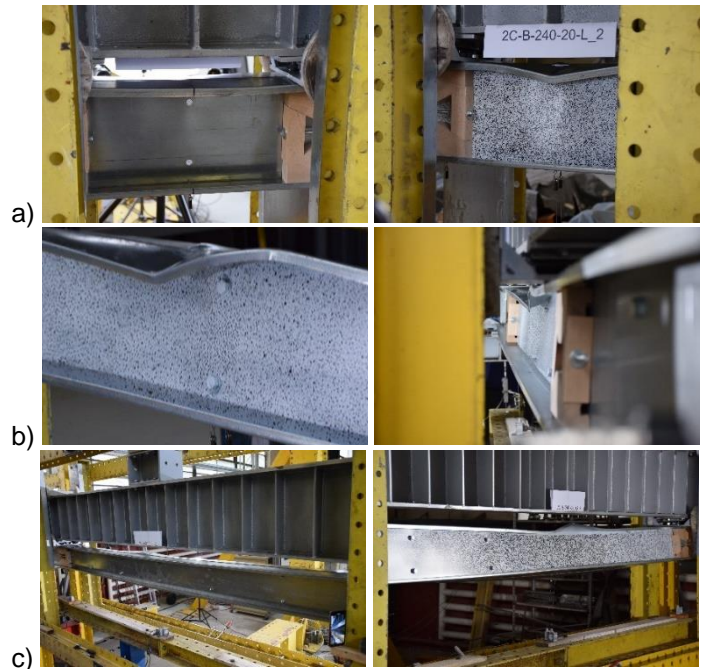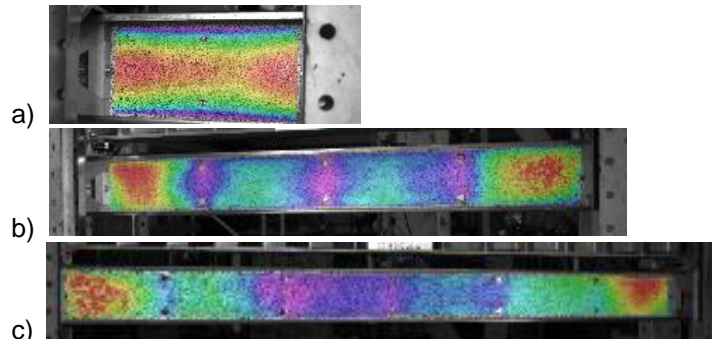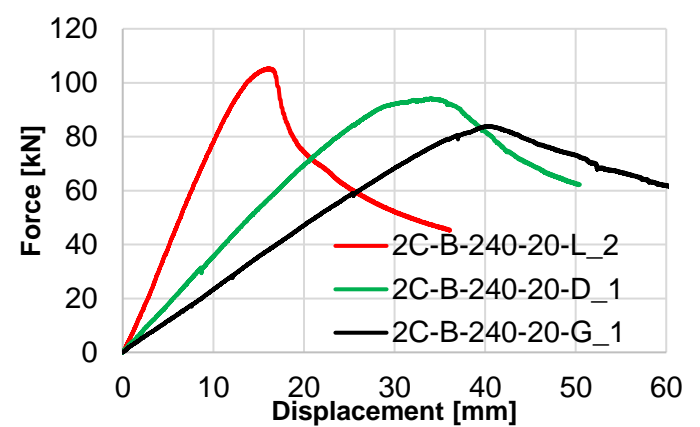
3.2 Built-up beams with spot welds of C200x1.5 profiles

Figure 14: Deformations for 2C-SW-200-1.5 a) Local, b) Distortional, c) Interactive buckling
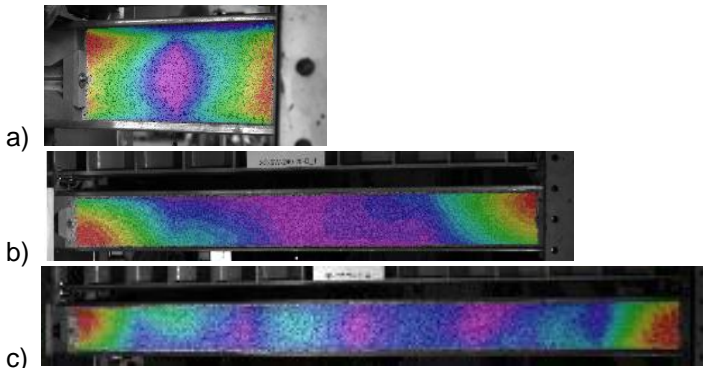

Figure 15: Initial imperfections for 2C-SW-200-1.5 a) Local, b) Distortional, c) Interactive buckling

Figure 16: Force-Displacement curves for 2C-SW-200-1.5

6

3.3 Built-up beams with bolts of C200x1.5 profiles and stitches

Figure 17: Deformations for 2C-St-B-200-1.5 a) Local, b) Distortional, c) Interactive buckling

Figure 18: Initial imperfections for 2C-St-B-200-1.5 a) Local, b) Distortional, c) Interactive buckling

Figure 19: Force-Displacement curves for 2C-St-B-200-1.5

3.4 Built-up beams with bolts of C240x2.0 profiles

Figure 20: Deformations for 2C-B-240-2.0 a) Local, b) Distortional, c) Interactive buckling

Figure 21: Initial imperfections for 2C-B-240-2.0 a) Local, b) Distortional, c) Interactive buckling

Figure 22: Force-Displacement curves for 2C-B-240-2.0

3.5 Built-up beams with spot welds of C240x2.0 profiles

Figure 23: Deformations for 2C-SW-240-2.0 a) Local, b) Distortional, c) Interactive buckling

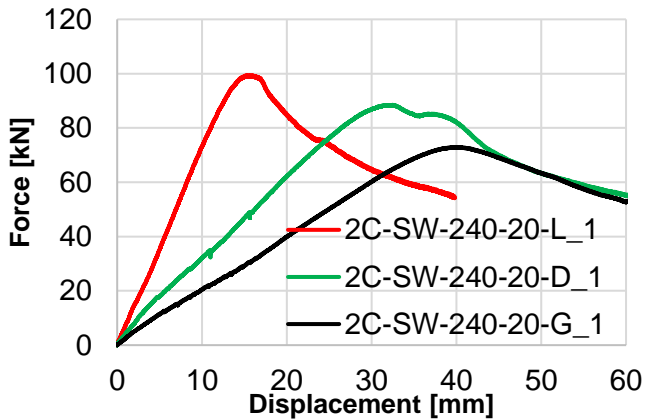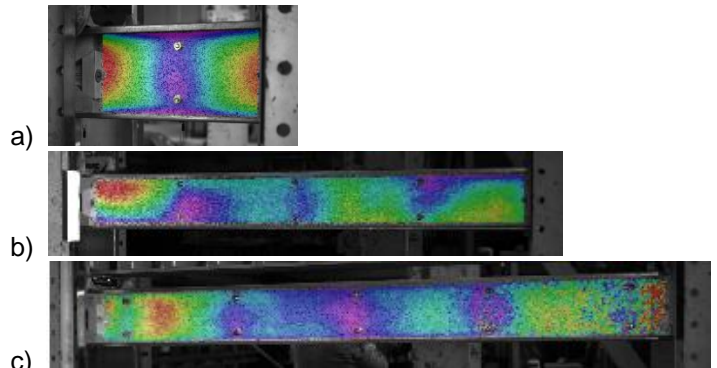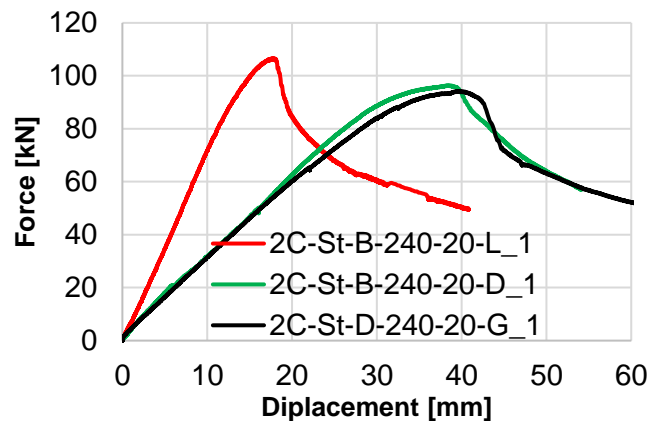Figure 24: Initial imperfections for 2C-SW-240-2.0 a) Local, b) Distortional, c) Interactive buckling

Figure 25: Force-Displacement curves for 2C-SW-240-2.0

3.6 Built-up beams with bolts of C240x2.0 profiles and stitches

Figure 26: Deformations for 2C-St-B-240-2.0 a) Local, b) Distortional, c) Interactive buckling

Figure 27: Initial imperfections for 2C-St-B-240-2.0 a) Local, b) Distortional, c) Interactive buckling

Figure 28: Force-Displacement curves for 2C-St-B-240-2.0

3.7 Built-up beams with bolts of U200x1.5 profiles

Figure 29: Deformations for 2U-B-200-1.5 a) Local, b) Interactive (Local+Global) buckling
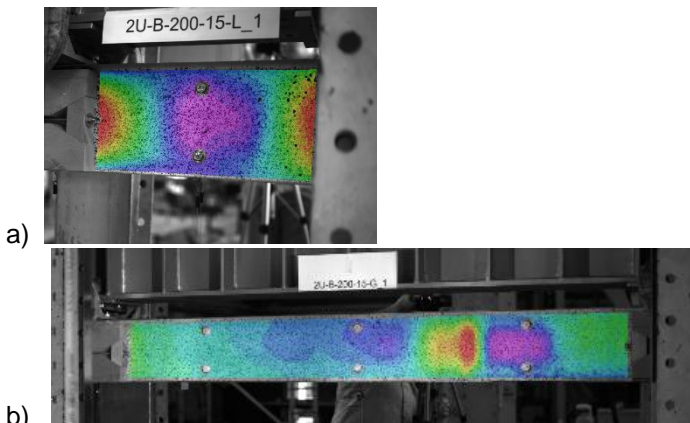

Figure 30: Initial imperfections for 2U-B-200-1.5 a) Local, b) Interactive (Local+Global) buckling
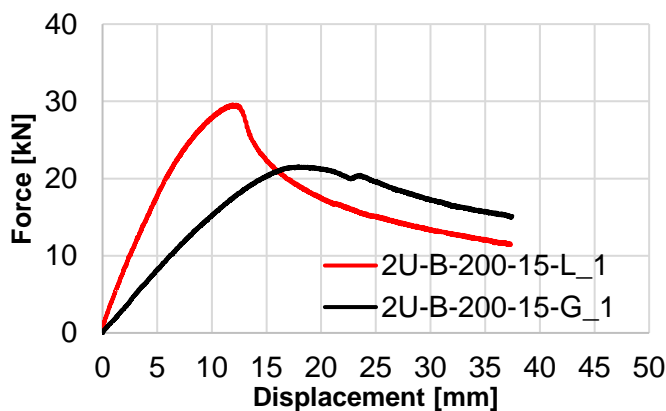

Figure 31: Force-Displacement curves for 2U-B-200-1.5

3.8 Built-up beams with spot welds of U200x1.5 profiles

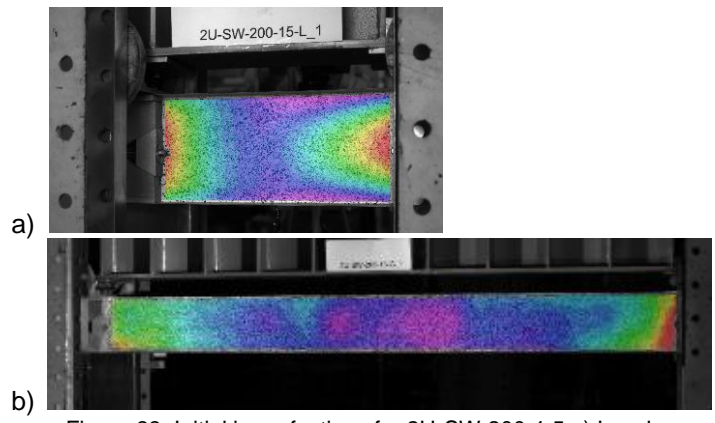Figure 32: Deformations for 2U-SW-200-1.5 a) Local, b) Interactive (Local+Global) buckling

Figure 33: Initial imperfections for 2U-SW-200-1.5 a) Local, b) Interactive (Local+Global) buckling
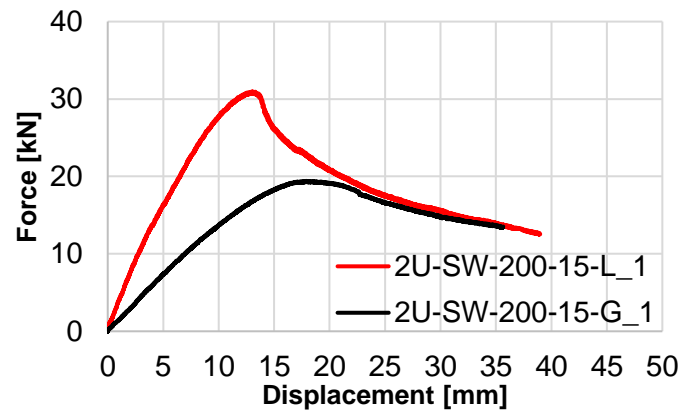

Figure 34: Force-Displacement curves for 2U-SW-200-1.5

For long plain channel section profiles (U profiles), in the first step, multiple half-wave lengths were visible that interact with the global buckling and transform into an interactive local-global buckling, see, e.g., Figure 35b), Figure 38 b).

For specimens with stitches between the single elements, the profiles exhibited interactive buckling, but the failure shape of the parts is independent, with both profiles showing an inward deformation of the compressed flange.

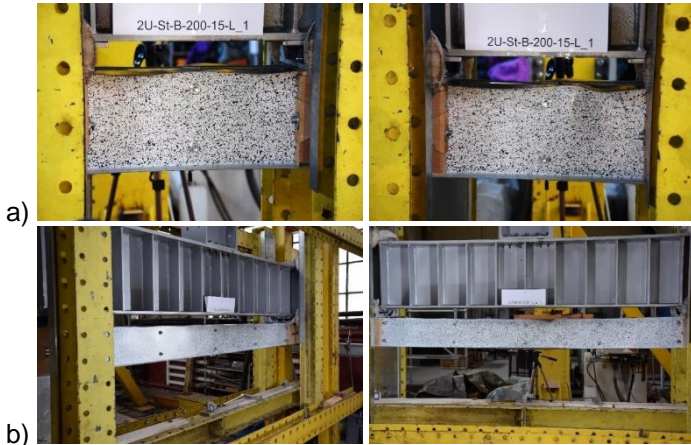## 3.9 Built-up beams with bolts of U200x1.5 profiles and stitches

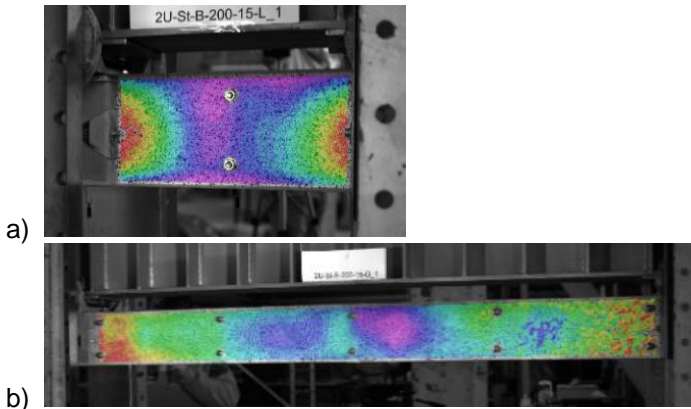Figure 35: Deformations for 2U-St-B-200-1.5 a) Local, b) Interactive (Local+Global) buckling

Figure 36: Initial imperfections for 2U-St-B-200-1.5 a) Local, b) Interactive (Local+Global) buckling
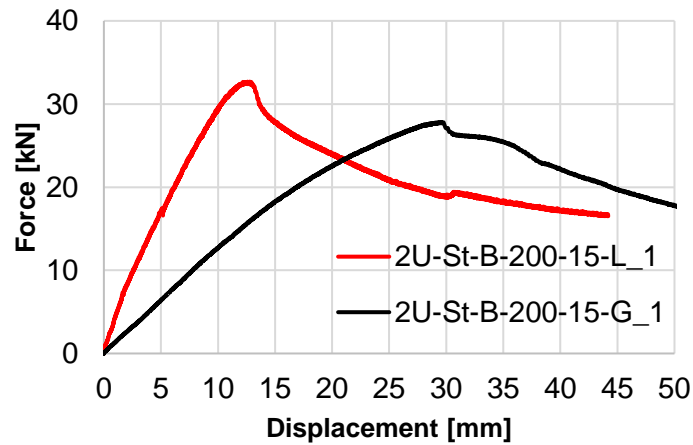

Figure 37: Force-Displacement curves for 2U-St-B-200-1.5

3.10 Built-up beams with bolts of U240x2.0 profiles

Figure 38: Deformations for 2U-B-240-2.0 a) Local, b) Interactive (Local+Global) buckling
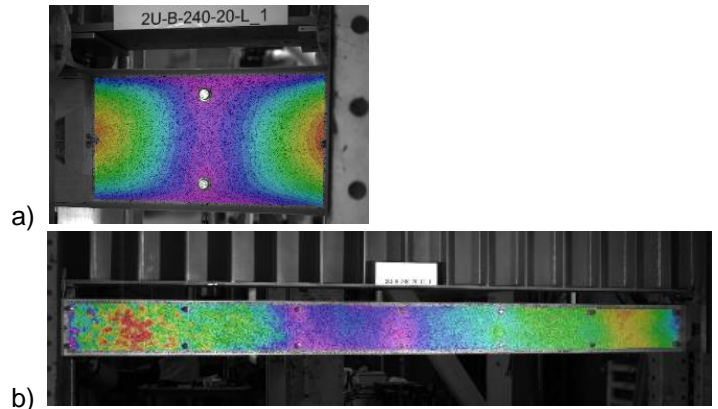

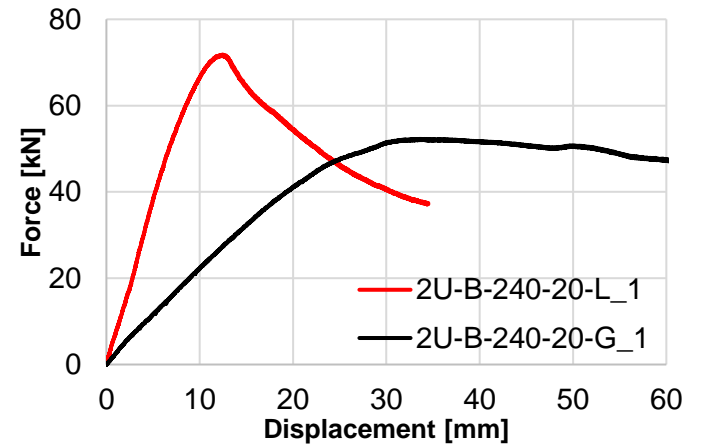Figure 39: Initial imperfections for 2U-B-240-2.0 a) Local, b) Interactive (Local+Global) buckling

Figure 40: Force-Displacement curves for 2U-B-240-2.0

3.11 Built-up beams with spot welds of U240x2.0 profiles

Figure 41: Deformations for 2U-SW-240-2.0 a) Local, b) Interactive (Local+Global) buckling
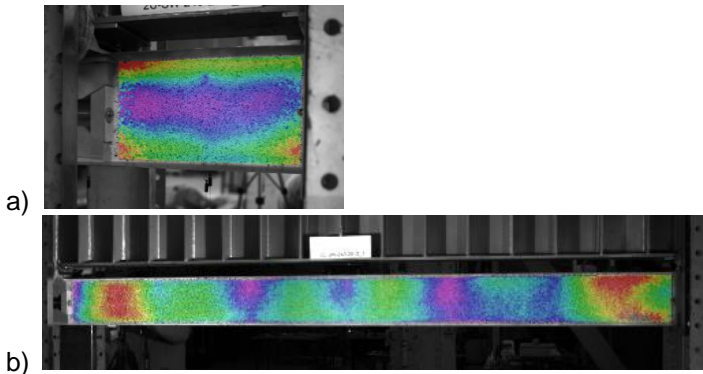

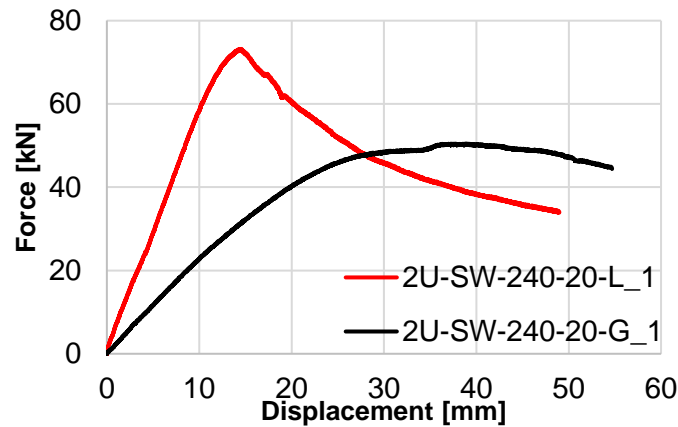Figure 42: Initial imperfections for 2U-SW-240-2.0 a) Local, b) Interactive (Local+Global) buckling

Figure 43: Force-Displacement curves for 2U-SW-240-2.0

In terms of capacity, the use of stitches did not result in a significant increase in flexural strength, not even for long specimens susceptible to global buckling.

3.12 Built-up beams with bolts of U240x2.0 profiles and stitches

Figure 44: Deformations for 2U-St-B-240-2.0 a) Local, b) Interactive (Local+Global) buckling
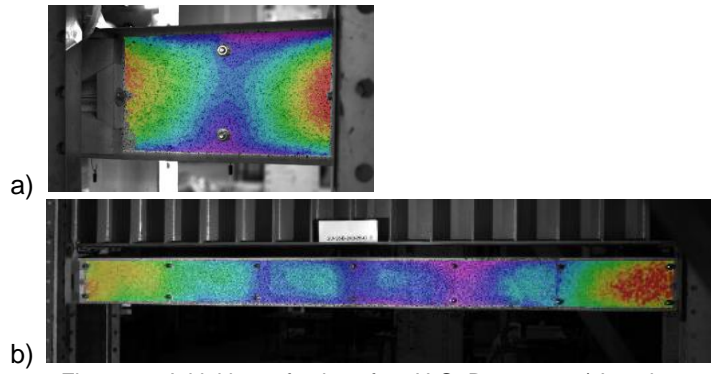

Figure 45: Initial imperfections for 2U-St-B-240-2.0 a) Local, b) Interactive (Local+Global) buckling
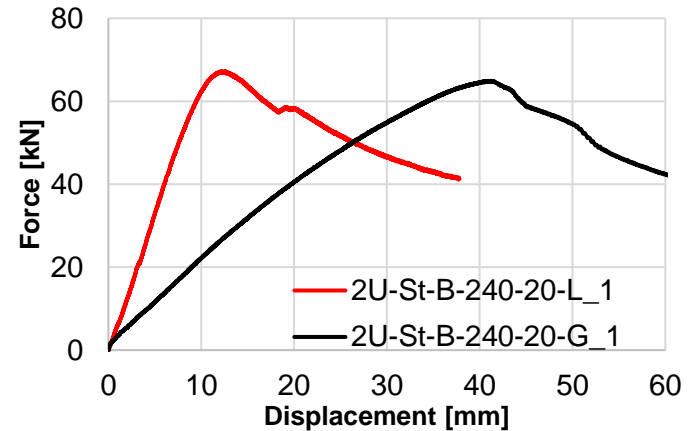

Figure 46: Force-Displacement curves for 2U-St-B-240-2.0

4. Conclusions

Plain and lipped channel sections commonly used in the European cold-formed steel construction sector were selected for the experimental study. Thirty thin-walled cold-

formed steel built-up beams made of lipped or plain channels, such as simple built-up back-to-back (SBB) and back-to-back with spacers (BBS) cross-sections, two types of discrete connections (bolts and spot welding) and various lengths were tested under bending to explore the behaviors of these members. The experimental study provided the details of failure modes, ultimate capacities, and force versus displacement curves. It showed that all short specimens primarily failed in interactive local buckling for members made of plain channels, while for lipped channels local-distortional interaction and pure distortional failure modes was recorded. For bigger lengths, interactive buckling was observed. The experimental investigation will be followed by finite element analyses throughout parametric studies and an improved design method for calculating the ultimate capacity of built-up open sections, promoting its use by design engineers and enabling economical and safer designs.

Table 8: Maximum bending moments supported by the specimen

Specimen	M_{max} (kNm)	Failure mode
2C-B-200-15-D	20.01	Distortional
2C-B-200-15-G	19.88	Interactive
2C-B-200-15-L	20.12	Local
2C-B-240-20-D	47.10	Distortional
2C-B-240-20-G	41.96	Interactive
2C-B-240-20-L	53.27	Local
2C-SW-200-15-D	19.80	Distortional
2C-SW-200-15-G	16.10	Interactive
2C-SW-200-15-L	21.01	Local
2C-SW-240-20-D	44.28	Distortional
2C-SW-240-20-G	40.16	Interactive
2C-SW-240-20-L	49.69	Local
2C-St-B-200-15-D	19.47	Distortional
2C-St-B-200-15-G	19.02	Interactive
2C-St-B-200-15-L	21.45	Local
2C-St-B-240-20-D	48.18	Distortional
2C-St-B-240-20-G	47.12	Interactive
2C-St-B-240-20-L	53.30	Local
2U-B-200-15-G	10.79	Interactive
2U-B-200-15-L	14.80	Local
2U-B-240-20-G	26.15	Interactive
2U-B-240-20-L	35.91	Local
2U-SW-200-15-G	12.37	Interactive
2U-SW-200-15-L	15.48	Local
2U-SW-240-20-G	25.23	Interactive
2U-SW-240-20-L	36.60	Local
2U-St-B-200-15-G	13.91	Interactive
2U-St-B-200-15-L	16.35	Local
2U-St-B-240-20-G	34.27	Interactive
2U-St-B-240-20-L	33.64	Local

References
[1] Stone, T.A. and LaBoube R.A. (2005). Behavior of cold-formed steel built-up I-sections. *Thin-Walled Structures*, vol. 43, no. 12, 1805–1817.
[2] Phan, D.K., Rasmussen, K.J. and Schafer, B.W. (2021). Tests and design of built-up section columns. *Journal of Constructional Steel Research*, 181, 106619.
[3] Phan, D.K., Rasmussen, K.J. and Schafer, B.W., (2022). Numerical investigation of the strength and design of cold-formed steel built-up columns. *Journal of Constructional Steel Research*, 193, 107276.
[4] Mahar, A.M., Arul Jayachandran, S. and Mahendran, M. (2022). Design of locally buckling cold-formed steel built-up columns formed by unlipped channel sections. *Thin-Walled Structures*, 174, 109132.
[5] Craveiro, H.D., Rahnavard, R., Laím, L., Simões, R.A. and Santiago, A. (2022). Buckling behavior of closed built-up cold-formed steel columns under compression. *Thin-Walled Structures*, 179, 109493.
[6] Li, Y., Zhou, T., Zhang, L., Ding, J. and Zhang X. (2021). Distortional buckling behavior of cold-formed steel built-up closed section columns. *Thin-Walled Structures*, 166, 10806.
[7] Li, Q.-Y. and Young, B. (2021). Tests of cold-formed steel built-up open section members under eccentric compressive load. *Journal of Constructional Steel Research*, 184, 106775.
[8] Ye, J., Hajirasouliha, I. and Becque, J. (2018). Experimental investigation of local-flexural interactive buckling of cold-formed steel channel columns. *Thin-Walled Structures*, 125, 245-258.
[9] Ye, J., Mojtabaei, S.M., Hajirasouliha, I., Shepherd, P. and Pilakoutas, K. (2018). Strength and deflection behaviour of cold-formed steel back-to-back channels. *Engineering Structures*, 177, 641–654.
[10] Li, Q.Y. and Young, B. (2022). Experimental study on cold-formed steel built-up section beam-columns experiencing non-uniform bending. *Engineering Structures*, 256, 113954.
[11] AISI S100-16, North American Specification for the Design of Cold-Formed Steel Structural Members. Washington, DC, U.S.A., AISI, 2016
[12] AS/NZS 4600, Design of cold-formed steel structures. Standards Australia and Standards New Zealand, Sydney, Australia, 2018.
[13] EN 1993-1-3, Eurocode 3: Design of Steel Structures, Part 1.3: General Rules. Supplementary Rules for Cold-formed Thin Gauge Members and Sheeting. Brussels, Belgium, CEN, 2006.
[14] ANSI/AISC 360-16, Specification for structural steel buildings. Chicago, U.S.A., AISI, 2016.
[15] Lukačević, I., Ungureanu, V., Valčić, A. and Ćurković, I. (2021). Numerical study on bending resistance of cold-formed steel back-to-back built-up elements. Special Issue: EUROSTEEL 2021 Sheffield - Steel's coming home. ce/papers, 4(2-4), 487-494.
[16] EN ISO 6892-1, Metallic materials - tensile testing. Part 1: Method of test at room temperature. Brussels, Belgium, CEN, 2009.